

Passive Assay of Plutonium Metal Plates using a Fast-Neutron Multiplicity Counter

D. L. Chichester, S. A. Pozzi, A. Di Fulvio,
T. H. Shin, T. Jordan, C. Sosa, M. L.
Ruch, S. D. Clarke

May 2017



The INL is a U.S. Department of Energy National Laboratory
operated by Battelle Energy Alliance

Passive Assay of Plutonium Metal Plates using a Fast-Neutron Multiplicity Counter

D. L. Chichester, S. A. Pozzi, A. Di Fulvio, T. H. Shin, T. Jordan, C. Sosa, M. L. Ruch, S. D. Clarke

May 2017

**Idaho National Laboratory
Idaho Falls, Idaho 83415**

<http://www.inl.gov>

**Prepared for the
U.S. Department of Energy
National Nuclear Security Administration
Under DOE Idaho Operations Office
Contract DE-AC07-05ID14517**

1 Passive Assay of Plutonium Metal Plates using a Fast-Neutron 2 Multiplicity Counter

3 A. Di Fulvio¹, T. H. Shin¹, T. Jordan¹, C. Sosa¹, M. L. Ruch¹, S.D. Clarke¹, D. L. Chichester², S. A. Pozzi¹

4 ¹Department of Nuclear Engineering & Radiological Sciences, University of Michigan, Ann Arbor MI 48109 U.S.A.

5 ²Idaho National Laboratory, Idaho Falls, ID 83415 U.S.A.

6 Abstract

7 We developed a fast-neutron multiplicity counter based on organic scintillators (EJ-309 liquid and
8 stilbene). The system detects correlated photon and neutron multiplets emitted by fission reactions,
9 within a gate time of tens of nanoseconds. The system was used at Idaho National Laboratory to assay a
10 variety of plutonium metal plates. A coincidence counting strategy was used to quantify the ²⁴⁰Pu
11 effective mass of the samples. Coincident neutrons, detected within a 40-ns coincidence window, show
12 a monotonic trend, increasing with the ²⁴⁰Pu-effective mass (in this work, we tested the 0.005-0.5 kg
13 range). After calibration, the system estimated the ²⁴⁰Pu effective mass of an unknown sample (²⁴⁰Pu_{eff}
14 >50 g) with an uncertainty lower than 1% in a 4-minute assay time.

15 1. Introduction and motivation

16 Nuclear materials accounting for safeguards applications often requires the non-destructive assay (NDA)
17 of plutonium-bearing materials, such as plutonium metal samples, metallic or oxide fuel rods, cans of
18 plutonium-oxide or mixed-oxide (containing both uranium and plutonium) powder, or scrap/waste
19 materials. Passive neutron coincidence counting is the technique of choice for this application, relying
20 on thermal neutron well counters [1]. A thermal-neutron well counter consists of a ring of ³He-based
21 proportional counters, embedded in a cadmium-lined polyethylene assembly. ³He-based well counters
22 are nearly insensitive to gamma-rays and have a relatively high intrinsic neutron detection efficiency
23 (10-30%) [2,3]. However, the coincidence gate is constrained by the relatively long neutron die-away
24 time (10 - 300 μ s) for these moderated detector assemblies [4], which is related to the neutron lifetime
25 in the system. Because of this long time-gate, the rate of accidental coincidences due to source and
26 random background events is rather large [5]. Thus, the main practical limitation of thermal systems is
27 the long measurement time required to overcome the large uncertainty in the counting statistics.

28 Organic scintillators detect both gamma-rays and fast neutrons, and can discriminate between the two
29 using pulse shape discrimination (PSD). Neutron detection in organic scintillators mostly relies on elastic
30 scattering on hydrogen nuclei. Because this reaction has a large cross-section for fast neutrons, no
31 moderation is required in systems using these detectors. Consequently, the neutron lifetime within the
32 system is of the order of tens of nanoseconds, which is several orders of magnitude shorter compared to
33 the neutron lifetime in thermal neutron counters. This feature makes it possible to reduce the
34 coincidence window by approximately three orders of magnitude in fast systems, compared to thermal
35 systems, resulting in significantly lower statistical measurement uncertainty [6,7].

36 In this work, we report the development and experimental validation of a fast-neutron multiplicity
37 counter (FNMC), based on sixteen organic scintillation detectors. The FNMC was used at Idaho National
38 Laboratory (INL) to passively assay two sets of plutonium metal plates, hereafter referred to as PAHN
39 and PANN. Each plate had a total mass of approximately 100 g, but different isotopic composition (74%
40 and 95% ^{239}Pu mass percentage, for PAHN and PANN series, respectively). The overall ^{240}Pu -effective
41 ($^{240}\text{Pu}_{\text{eff}}$) mass of the measured assemblies of plates was in the 4.7 g - 476 g range. To quantify the
42 $^{240}\text{Pu}_{\text{eff}}$ mass of the samples, we calibrated the system response using a subset of the results, and then
43 measured the neutron doubles rate emitted by the remaining samples.

44 2. Materials and Methods

45 2.1 Detectors and readout electronics

46 The FNMC consists of eight liquid organic scintillators (EJ-309, 7.62-cm diameter by 7.62-cm length, by
47 Eljen, Sweetwater, Tex.) and eight stilbene detectors (5.08-cm diameter by 5.08-cm length, by Lawrence
48 Livermore National Laboratory and Inrad Optics, Northvale, N.J.). The detectors were in an alternating
49 arrangement, so that two detectors of the same type were never next to each other, either in the top or
50 bottom layer (Fig. 1). EJ-309 and stilbene feature similar elemental composition (Table 1) and are both
51 PSD-capable organic scintillators. PSD performance of the detectors is critical in this application, where
52 fission neutrons from 0.1 to several MeV must be detected in the presence of an intense gamma-ray
53 background.

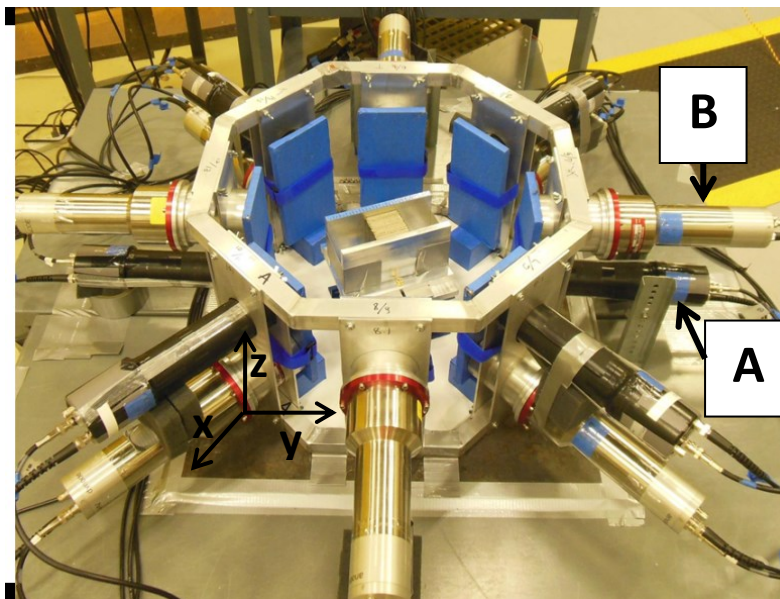


Figure 1. Stilbene (A) and EJ-309 (B) based Fast Neutron Multiplicity Counter at INL while measuring 19 plutonium metal plates.

54

55

56

57

58

59

Table 1. Properties of EJ-309 and stilbene detectors.

60

	EJ-309 [8]	Stilbene
Chemical formula	n. a.	C ₁₄ H ₁₂
Geometric isomerism	n. a.	Trans
H:C ratio	1.25	0.86
Light output (% anthracene)	80	64, 69*
Maximum wavelength (nm)	424	390
Scintillation efficiency (photons/ 1 MeVee)	12300	9670**
Fast decay time constant (ns)	3.5	4.5**
Flash point (°C)	144	n. a.
Size (length, cm; diameter, cm)	7.62;7.62	5.08; 5.08
Photomultiplier tube (model; manufacturer)	9214B; ET Enterprises Ltd (Uxbridge, UK)	9214B; ET Enterprises Ltd (Uxbridge, UK)

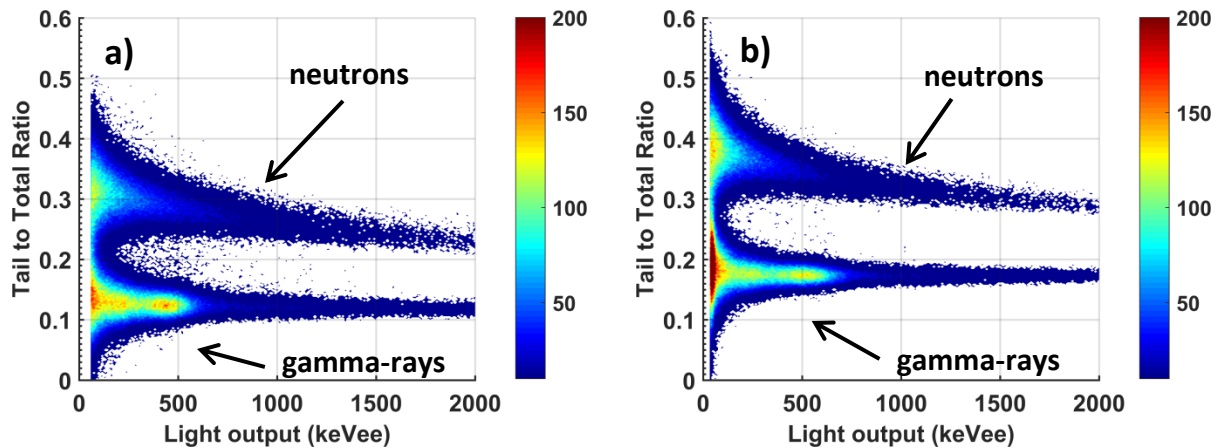
68

69 * Relative light output refers to solution-grown stilbene, compared to two anthracene crystals with
70 different structural perfections [9].

71 ** This value refers to melt-grown stilbene [5][10], solution-grown crystal is expected to outperform the
72 scintillation efficiency figure by about 50%[9].

73 Pulses were acquired and directly converted to digital waveforms using a 500-MS/s, 14-bit, 16-channel
74 digitizer (V1730 by CAEN Technologies, Viareggio, Italy [11]). We performed pulse shape discrimination
75 using a standard charge integration method [12].

76



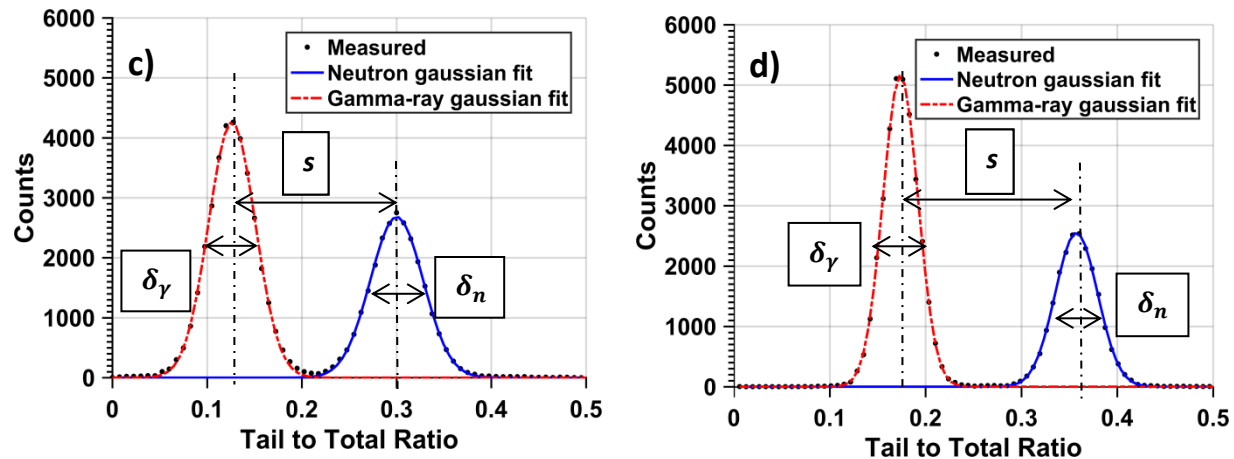


Figure 2. PSD analysis for an EJ-309 (a) and a stilbene detector (b). PSD plots correspond to detector irradiation with one of the plutonium metal samples. Count distribution as a function of the tail to total ratio for 100-200 keVee light output, for EJ-309 (c) and stilbene (d).

77

78 This method is based on the delayed-fluorescence component, selectively emitted after scintillator
 79 interactions with high-LET charged particles, e.g., recoil protons produced by neutron scattering [13].
 80 Therefore, neutron-induced pulses exhibit an overall slower decay constant, compared to photon-
 81 generated pulses. The charge integration method estimates the energy deposited in the tail of each
 82 pulse, relative to the total pulse energy, to discriminate between photon and neutron pulses. We found
 83 that the tail start time for an optimized PSD was 24 ns after the pulse peak.

84 The ratio between the pulse tail and pulse total integral (tail-to-total ratio) as a function of the total
 85 pulse integral, in light output units, for 5×10^5 detected pulses, is shown in Fig. 2a and Fig. 2b. A figure of
 86 merit (FOM) value is typically used to characterize the scintillator PSD performance. The FOM can be
 87 defined as $s/(\delta_n + \delta_\gamma)$, where s is the separation between the peaks of the neutron and gamma-ray
 88 distributions (Fig 2c-d), at a given light output, and δ_n and δ_γ are the full-widths at half-maximum of the
 89 neutron and gamma-ray bands, respectively (Fig. 2c, Fig. 2d).

90 The system achieved a readout rate of approximately 60 MBps, with a negligible dead-time,
 91 corresponding to approximately 140,000 waveforms per second. For some of the plutonium metal
 92 assemblies the trigger rate exceeded the maximum readout rate, mainly because of the highly-
 93 radioactive ^{241}Am present in the fuel from the decay of ^{241}Pu [14]. Therefore, we implemented an
 94 acquisition-in-coincidence readout logic, which drastically reduced the readout throughput due to
 95 random background pulses. This acquisition-in-coincidence readout logic accepts only those pulses
 96 which occur in coincidence within a window of programmable length (for this application, we used 40
 97 ns). This acquisition-in-coincidence strategy discards uncorrelated detection events. Furthermore, all the
 98 pulses detected in coincidence by top-bottom nearest neighbor detectors, e.g. detectors “A” and “B” in
 99 Fig. 1, were also rejected. This readout method is meant to reject most of the spurious coincidence
 100 events referred to as cross-talk events [15], which occur whenever a neutron is scattered from one

101 detector into another and deposits enough energy to be detected in both of them. In order to compare
102 the two acquisition methods, a few assemblies were measured using both the singles and the
103 coincidence acquisition mode. In the case of a single PAHN case, for example, the count rate in
104 coincidence mode was approximately 1% and 0.08% of the count rate in singles mode, for neutrons
105 and photons, respectively.

106 Prior to the experiment, the detectors were gain-matched using a $0.1\text{-}\mu\text{Ci }^{137}\text{Cs}$ source. We used a $25\text{-}\mu\text{Ci }^{252}\text{Cf}$
107 source to optimize the detection threshold. It is desirable to operate the detectors at a low
108 energy threshold to maximize the neutron-detection efficiency. However, as the threshold decreases,
109 the number of gamma-ray pulses that are misclassified as neutron pulses unavoidably increases.
110 Considering this effect, we selected a detection threshold such that the misclassification rate of gamma-
111 ray pulses was lower than 10^{-6} per detection [12]. Due to the superior PSD performance of stilbene, the
112 detection threshold of the stilbene detectors was set to 30 keVee, lower than the 50-keVee threshold
113 used for the EJ-309 detectors. These threshold settings provided a dynamic range of 30–2,400 keVee
114 (this corresponds to approximately 336–6,500 keV neutron energy deposited) for stilbene and 50–2,400
115 keVee (approximately 520–5,530 keV neutron energy deposited) for EJ-309. The maximum energy
116 deposited by a neutron scattering on hydrogen nuclei was derived using the Voltz model of the light
117 output function, fitted to EJ-309 [16] and stilbene[17] data by Norsworthy and colleagues [16]. The
118 selected readout range minimized the amount clipped pulses, while also amplifying low-amplitude
119 pulses, to improve PSD performance at low energies (< 200 keVee).

120 **2.2 Assay samples: plutonium metal plates**

121 Table 2 gives the isotopic composition of the two sets of metal plates [18], aged to the date of the
122 experiment, August 2015. These samples are fuel plates designed and built for the INL Zero Power
123 Physics Reactor (ZPPR). The external dimensions of a single plate are 7.62 cm by 5.08 cm (thickness
124 0.3175 cm). The plutonium metal core is encapsulated in a thin 304 L stainless steel cladding. Based on
125 the fuel element geometry [19], we estimate core densities of 15.08 g/cm^3 and 15.09 g/cm^3 , for PAHN
126 and PANN.

127 The $^{240}\text{Pu}_{\text{eff}}$ mass is defined as the mass of ^{240}Pu that would give the same response in terms of neutron
128 coincidences (doubles) as that obtained by the actual ^{238}Pu , ^{240}Pu and ^{242}Pu content of the sample. The
129 $^{240}\text{Pu}_{\text{eff}}$ mass for systems based on ^3He detectors is calculated as a linear combination of the masses of
130 the plutonium isotopes having even mass numbers, A (Eq. 1). The neutron coincidence rate is used to
131 estimate the sample $^{240}\text{Pu}_{\text{eff}}$ mass and depends on both the multiplicity distribution of the sample and
132 the efficiency of the system to detect multiplets of the second-order (i.e. neutron doubles). For this
133 reason, the multiplicative coefficients in Eq. 1 are expected to be different for fast and thermal systems.
134 Dolan and colleagues simulated the neutron coincidence response of a fast neutron multiplicity counter
135 based on 16 EJ-309 scintillators [20], very similar to our FNMC, and derived the $^{240}\text{Pu}_{\text{eff}}$ mass equation
136 coefficients, specific to their system. The PAHN and PANN $^{240}\text{Pu}_{\text{eff}}$ mass obtained using these coefficients
137 was not significantly different from the one calculated using the coefficients for thermal systems (Eq. 1),
138 which were then used in this work. The $^{240}\text{Pu}_{\text{eff}}$ mass for a single PANN and PAHN plate is 4.70 g and
139 25.05 g, respectively.

140 $^{240}\text{Pu}_{eff} = 2.49 \text{ }^{238}\text{Pu} + \text{}^{240}\text{Pu} + 1.57 \text{ }^{242}\text{Pu}$ 1

141

142 **Table 2. Isotopic composition of PAHN and PANN plates, August 2015. Isotope mass uncertainty was calculated taking into**
 143 **account the known uncertainty in the half-life of each isotope and the aging time.**

	PAHN mass (g)	PANN mass (g)
²³⁸ Pu	0.00020(7)	0.00023(6)
²³⁹ Pu	79.69(2)	98.89(2)
²⁴⁰ Pu	23.92(1)	4.70(1)
²⁴¹ Pu	0.65(1)	0.04(1)
²⁴² Pu	0.67(1)	<0.009
²⁴¹ Am	1.87(1)	0.23(1)
Al	1.25	1.16
Total plutonium	106.79	103.87

144

145

146 Actinide decay in the PAHN and PANN fuels produces overall gamma-ray emission rates of $8.1 \times 10^{10} \text{ s}^{-1}$
 147 and $1.1 \times 10^{10} \text{ s}^{-1}$, respectively. The higher gamma-ray activity of PAHN plates, with respect to PANN, is
 148 due to its higher ²⁴¹Pu and ²⁴⁰Pu mass content, and thus higher ²⁴¹Am content [14]. Although the energy
 149 of these gamma rays is relatively low (<700 keV), their intensity may be problematic, especially when
 150 lowering the energy threshold of the scintillators to increase the neutron detection efficiency. The
 151 neutron emission rates for the PAHN and PANN are 1.17×10^4 and $2.20 \times 10^3 \text{ s}^{-1}$, respectively. The gamma-
 152 ray/neutron ratio detected by the scintillators, which are shielded by 1.2 cm-thick lead plates (Fig. 1), is
 153 about 65 for the PAHN and 40 for the PANN in singles mode, and approximately 4 in coincidence mode,
 154 for both types of plate.

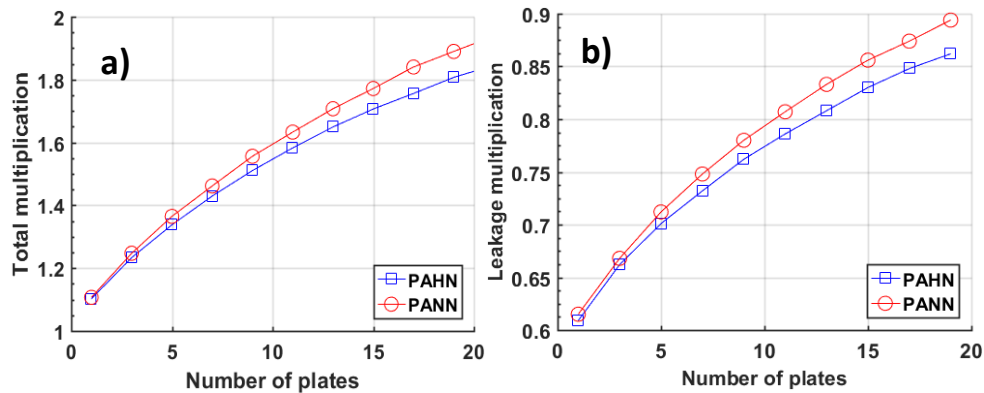


Figure 3. Simulated total multiplication (a) and leakage multiplication (b) for PAHN and PANN plate assemblies of 1-19 plates.

155 A multiplicity counter is sensitive to the multiplicity of the fission events. The neutron multiplication M
 156 characterizes the dynamics of the fission neutron population of a finite multiplying system. The neutron
 157 multiplication is calculated as the number of neutrons in the sample, divided by the first-generation
 158 neutron population. The neutron multiplication was simulated for subcritical assemblies of up to 19
 159 plates of PAHN and PANN plates (Fig. 3a). The leakage multiplication, M_L , is the measureable
 160 multiplication and it is defined as the ratio between the number of neutrons leaving the sample and the
 161 number of neutrons produced within the sample, by spontaneous and induced fission in the case of
 162 plutonium metal samples (Fig. 3b).

163 The $^{240}\text{Pu}_{\text{eff}}$ mass of a sample depends not only on its mass, but also on the multiplication. Samples with
 164 the same mass and elemental composition, but with different multiplication due to, for example, a
 165 different geometric configuration, may yield a different $^{240}\text{Pu}_{\text{eff}}$ mass. The current system operates in
 166 coincidence mode: $^{240}\text{Pu}_{\text{eff}}$ mass estimate relies on the rate of neutron pairs detected in coincidence.
 167 Therefore, the estimate of $^{240}\text{Pu}_{\text{eff}}$ mass for samples with different mass and multiplication poses an
 168 undetermined problem. It is therefore necessary to either correct for the neutron multiplication [1], or
 169 to derive, experimentally or via simulation, a system response curve, in terms of $^{240}\text{Pu}_{\text{eff}}$ mass, for each
 170 sample composition to be assayed. In this work, we demonstrate both approaches.

171 2.3 Single-parameter calibration procedure and uncertainty estimation

172 The coincidence counting system was first calibrated in single-parameter mode by measuring the
 173 coincidence rate, D , as a function of $^{240}\text{Pu}_{\text{eff}}$ mass, for samples of known mass. The following procedure
 174 was used to derive the calibration curve and the uncertainty value associated to the estimated $^{240}\text{Pu}_{\text{eff}}$
 175 mass of unknown samples.

176 The most appropriate fit for the data was a polynomial relationship (Eq. 2). The least-squares fitting
 177 process gives an estimate of the model coefficients, a and b , and their variances: s_a^2 and s_b^2 [21].

$$178 \quad D = a \ ^{240}\text{Pu}_{\text{eff}}^2 + b \ ^{240}\text{Pu}_{\text{eff}} \quad 2$$

179 The $^{240}\text{Pu}_{\text{eff}}$ mass can be related to the measured coincidence count rate using the following expression
 180 (Eq. 3), once the calibration curve is established.

$$181 \quad ^{240}\text{Pu}_{\text{eff}} = \frac{(\sqrt{4aD+b^2}-b)}{2a} \quad 3$$

182 An uncertainty, u , can be assigned to the estimated mass by propagating the uncertainty through Eq. 3.
 183 The primary assumption is that each neutron double (pair of neutrons detected in coincidence) is the
 184 result of a single fission reaction and thus the uncertainty associated with the number of measured
 185 doubles can be modeled as a Poisson process and the variance of the count rate (s_D^2) is equal to its
 186 mean.

$$187 \quad u^2 = \left(\frac{\partial \ ^{240}\text{Pu}_{\text{eff}}}{\partial D}\right)^2 s_D^2 + \left(\frac{\partial \ ^{240}\text{Pu}_{\text{eff}}}{\partial a}\right)^2 s_a^2 + \left(\frac{\partial \ ^{240}\text{Pu}_{\text{eff}}}{\partial b}\right)^2 s_b^2 + 2\left(\frac{\partial \ ^{240}\text{Pu}_{\text{eff}}}{\partial a}\right)\left(\frac{\partial \ ^{240}\text{Pu}_{\text{eff}}}{\partial b}\right) s_{ab} \quad 4$$

188 In Eq. 4, s_{ab} is the covariance between the two coefficients a and b .

189 2.3 Two-parameter calibration procedure and uncertainty estimation

190 The two-parameter calibration approach aims at removing the effect of multiplication from the assay.
191 We constructed a calibration curve by plotting the ratio of double-to-single neutron count rate (D/S), as
192 a function of neutron coincidence rate per gram of $^{240}\text{Pu}_{\text{eff}}$ mass ($D/^{240}\text{Pu}_{\text{eff}}$). Because both D/S and
193 $D/^{240}\text{Pu}_{\text{eff}}$ depend on the sample multiplication, their relationship is expected to be linear (Eq. 5) for a
194 series of samples with the same contribution of (α, n) neutrons, which is estimated to be zero for the
195 INL plutonium metal plates.

$$196 \quad \frac{D}{S} = c \frac{D}{^{240}\text{Pu}_{\text{eff}}} + d \quad 5$$

197 After deriving the calibration curve, we measured D/S for the samples to be assayed and determined
198 their neutron coincidence rate per unit $^{240}\text{Pu}_{\text{eff}}$ mass ($K = \frac{D}{^{240}\text{Pu}_{\text{eff}}}$) from the calibration curve. Because
199 D can be measured, the value of $^{240}\text{Pu}_{\text{eff}}$ mass was simply calculated as D/K .

200 The uncertainty to be associated with the estimated $^{240}\text{Pu}_{\text{eff}}$ mass, u , is then derived using Eq. 6, with
201 analogous assumptions and procedures as for Eq. 4.

$$202 \quad u^2 =$$
$$203 \quad \left(\frac{\partial ^{240}\text{Pu}_{\text{eff}}}{\partial D}\right)^2 s_D^2 + \left(\frac{\partial ^{240}\text{Pu}_{\text{eff}}}{\partial S}\right)^2 s_S^2 + \left(\frac{\partial ^{240}\text{Pu}_{\text{eff}}}{\partial c}\right)^2 s_c^2 + \left(\frac{\partial ^{240}\text{Pu}_{\text{eff}}}{\partial d}\right)^2 s_d^2 +$$
$$204 \quad 2\left(\frac{\partial ^{240}\text{Pu}_{\text{eff}}}{\partial c}\right)\left(\frac{\partial ^{240}\text{Pu}_{\text{eff}}}{\partial d}\right) s_{cd} \quad 6$$

205 In Eq. 6, s_c^2 and s_d^2 are the variances associated with the calibration curve parameters, c and d ,
206 respectively, and s_{cd} is their covariance coefficient.

207

208 3. Results

209 3.1 Comparison of EJ-309 and stilbene PSD performance

210 Fig. 4 shows the FOM as a function of light output for pulses acquired for an assembly of 19 PANN
211 plates, for a stilbene and an EJ-309 detector. The FOM in Fig. 4 is calculated from scatter plots reported
212 in Fig. 2.a-b. The separation between the gamma-ray and neutron regions increases with light output,
213 generating an increasing trend in the FOM. The FOM is higher in the stilbene detector than in the EJ-309
214 liquid scintillation detector. This excellent stilbene PSD performance allows us to operate the detector at
215 a threshold as low as 30 keVee.

216

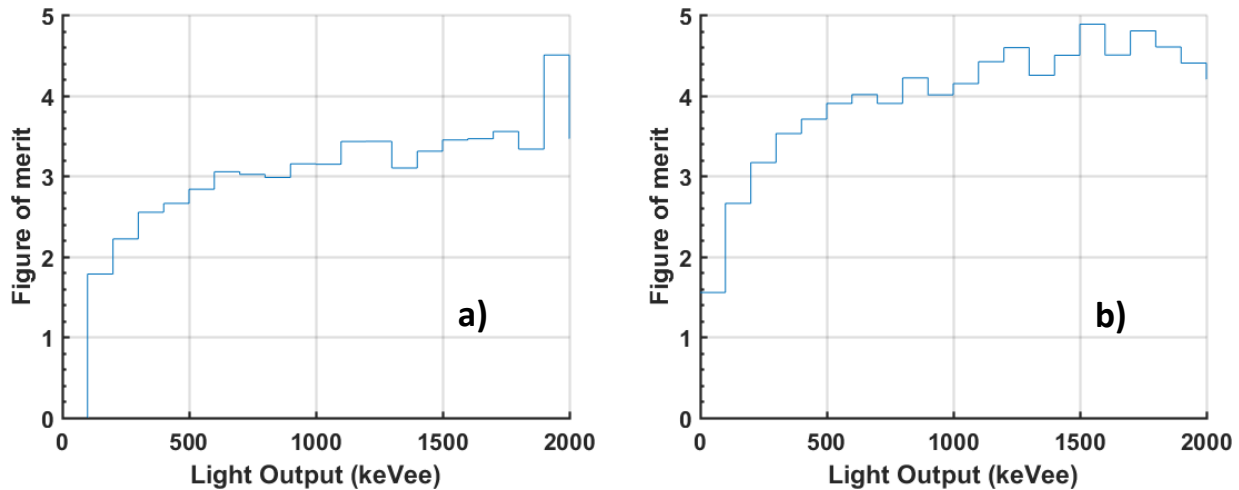
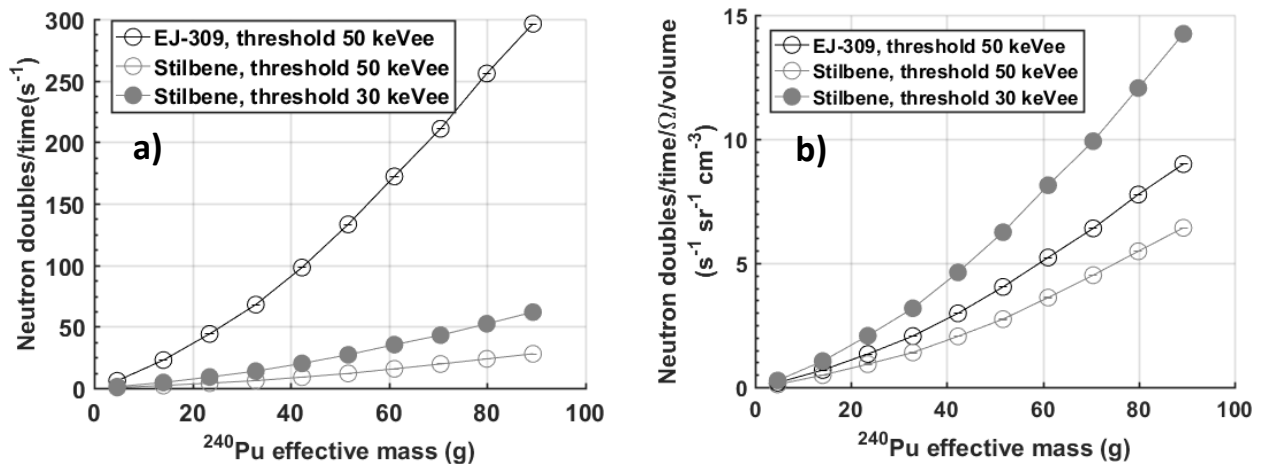


Figure 4. Figure-of-merit for an EJ-309 (a) and a stilbene detector (b), irradiated using 19 PANN plates.

217

218

219 Fig. 5 shows the count rate of neutron doubles as a function of $^{240}\text{Pu}_{\text{eff}}$ mass. Neutrons detected in
 220 coincidence by 8 EJ-309 and 8 stilbene detectors are shown separately. The lower absolute response of
 221 stilbene crystals, compared to EJ-309 detectors (Fig. 5a-c), is due to their smaller volume. However, the
 222 stilbene response, normalized by detector volume and detection solid angle, is consistently higher than
 223 the EJ-309 response by about 50% (Fig. 5b-d). The higher normalized detection efficiency of stilbene,
 224 compared to EJ-309, is due to the detection threshold, which is lower in stilbene (30 keVee), than in EJ-
 225 309 (50 keVee). If the scintillators were to be operated at the same threshold (Fig. 5b-d) the stilbene
 226 overall response would be lower than EJ-309 because of its lower light output (Table 2), negatively
 227 affected by quenching phenomena of the proton pulses [13].



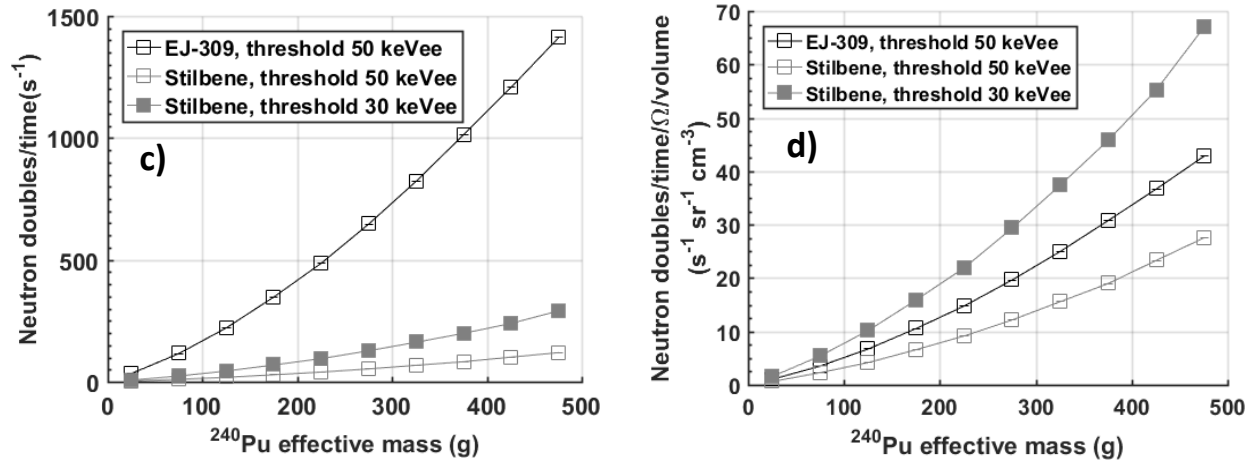


Figure 5. Count rate of neutron doubles per unit solid angle and volume as a function of the number of plates (PANN series: a, b and PAHN series: c, d). Stilbene and EJ309 contributions are separated (a, c) and normalized by volume and solid angle (b, d).

228 3.2 System simulation and cross-talk rejection

229 A model of the plutonium metal samples and the FNMC was developed in MCNPX-PoliMi [22] in
 230 preparation of the experiment. Fig. 6 shows the measured and simulated neutron multiplet rates for the
 231 two sets of plates. The goal of the simulation was to find the optimal detector-to-sample distance,
 232 sample orientation, and lead thickness to maximize the sensitivity to emitted neutron doubles as well as
 233 characterize the gamma-ray response. We used the MCNPX-PoliMi built-in spontaneous fission ^{240}Pu
 234 model, which simulates the energy distribution of the emitted neutrons as a function of the multiplicity,
 235 as well as an anisotropic angular distribution. The simulated and measured double rates generally agree
 236 well, while higher order simulated multiplets tend to overestimate the measurement. The effect of
 237 rejecting coincidence counts from top-bottom nearest neighbor detectors resulted in a decrease of the
 238 overall response by 8.9% and was considered in the simulation.

239 In principle, a neutron coincidence event may occur after a spallation reaction between high-energy
 240 charged particles, produced by cosmic rays, and the nuclei of a high-Z material. This effect was
 241 estimated to be negligible in our system. The rate of background double neutrons was measured as $<10^{-2}$
 242 s^{-1} in the ZPPR facility building; therefore, no background correction was applied.

243

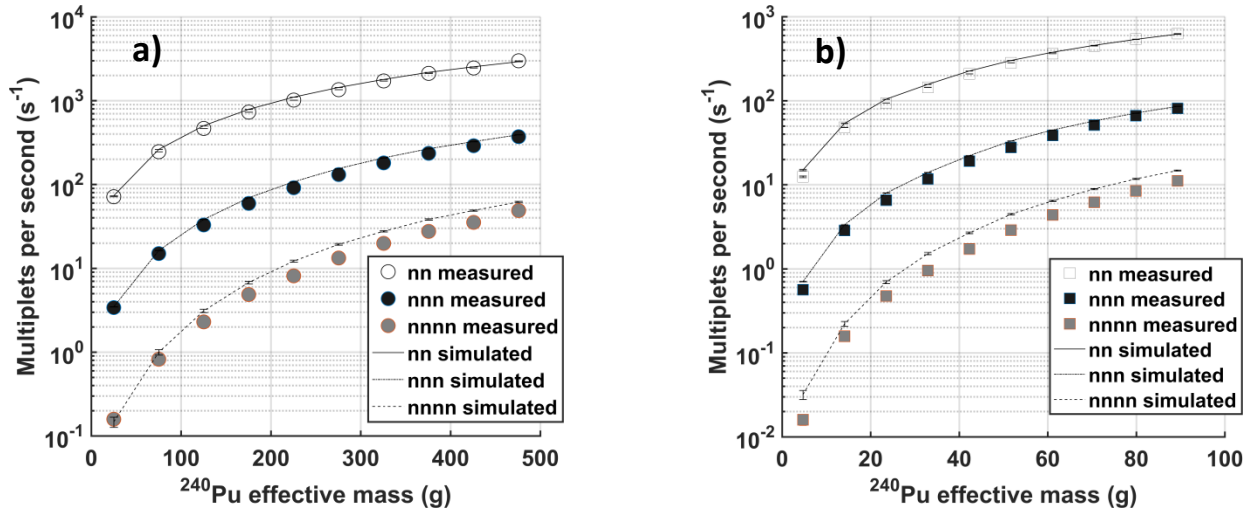


Figure 6. Simulated and measured rate of neutron multipliers as a function of $^{240}\text{Pu}_{\text{eff}}$ mass, for PAHN (a) and PANN plates (b).

244

245 3.3 Estimate of ^{240}Pu effective mass using single-parameter calibration

246

247 Assemblies of 3, 9 and 15 plates were used to build a calibration curve for each data set (Fig. 7a and
 248 Fig.8a). Assemblies of 1, 5, 7, 11, 13, 17, and 19 plates were used as a test set; their mass was assumed
 249 to be unknown and was estimated using Eq. 3. The process of measuring the unknown $^{240}\text{Pu}_{\text{eff}}$ mass of
 250 sample is exemplified by two arrows in Fig. 7b, for an assembly of 13 PANN plates. Fig. 7b and Fig. 8b
 251 show the estimated $^{240}\text{Pu}_{\text{eff}}$ mass using the single-parameter calibration procedure, compared to the
 252 known $^{240}\text{Pu}_{\text{eff}}$ mass for PANN and PAHN plate assemblies, respectively.

253 Table 3 shows the estimated values of $^{240}\text{Pu}_{\text{eff}}$ mass for the test-set plate assemblies and the
 254 uncertainties associated with them, u . The uncertainty was calculated using the technique in the
 255 previous section, and accounts for counting uncertainty and possible deficiencies of the fitting model in
 256 capturing all the information in the data.

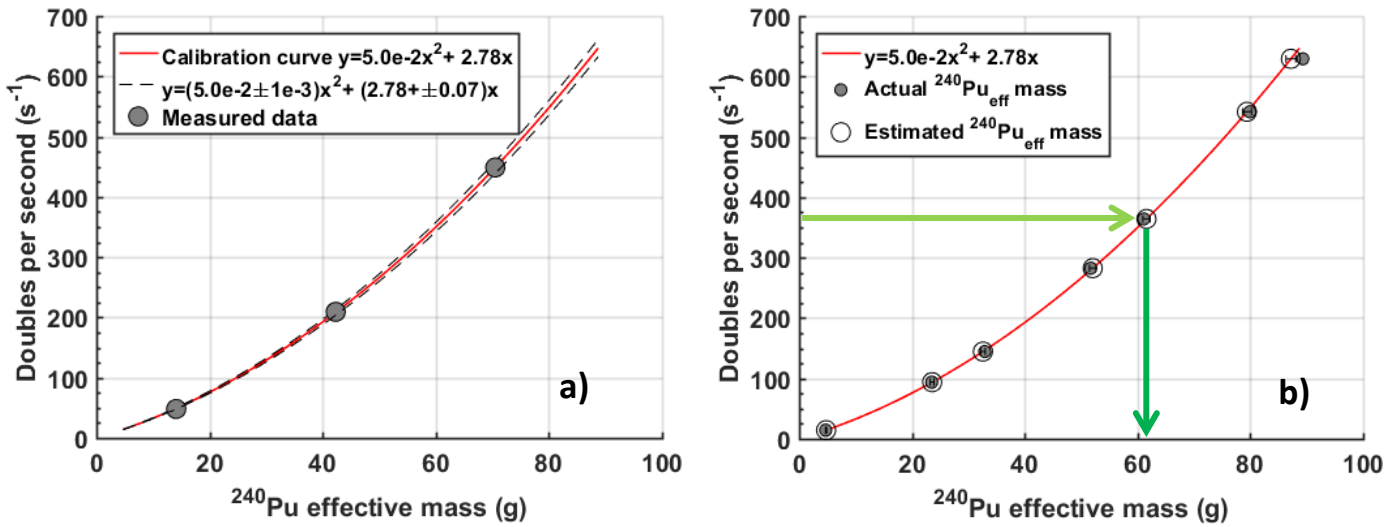


Figure 7. Fit of neutron doubles rate as a function of $^{240}\text{Pu}_{\text{eff}}$ mass to build the calibration curve (a) and validation of the calibration curve using assemblies of 1, 5, 7, 11, 13, 17, and 19 plates (b). Both graphs refer to PANN plates.

258 We also report the relative bias of the estimated $^{240}\text{Pu}_{\text{eff}}$ mass with respect to the known $^{240}\text{Pu}_{\text{eff}}$ mass.
 259 This relative difference should account for all the sources of systematic errors, including any drift in the
 260 system working conditions, which could systematically affect the measurement results. The bias error is
 261 always within $\pm 3u$, which proves that no significant bias can be identified during the system operation
 262 and the model explains well the intrinsic measurement uncertainty of the system.

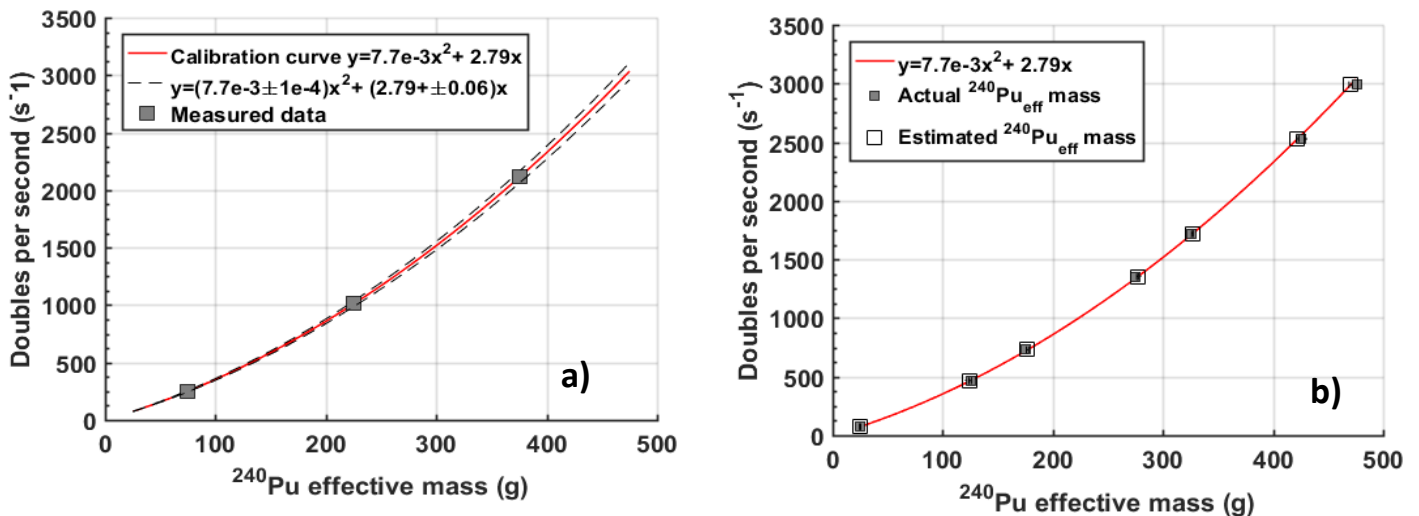


Figure 8. Fit of neutron doubles rate as a function of $^{240}\text{Pu}_{\text{eff}}$ mass to build the calibration curve (a) and validation of the calibration curve using assemblies of 1, 5, 7, 11, 13, 17, and 19 plates (b). Both graphs refer to PAHN plates.

264 We post-processed a subset of the data to study the dependence of the measurement statistical
 265 uncertainty as a function of the assay time. An uncertainty lower than 1% in the $^{240}\text{Pu}_{\text{eff}}$ mass was

266 achieved in a 4-minute assay time, for $^{240}\text{Pu}_{\text{eff}}$ masses higher than 50 g, as shown in Fig. 9. The
 267 percentage uncertainty is expected to be higher for smaller samples.

268 In a 4-minute assay, our system estimated a $^{40}\text{Pu}_{\text{eff}}$ mass of 4.78 ± 0.11 g and 23.58 ± 0.25 g (2.4% and
 269 1.1% relative uncertainty, respectively) for PANN assemblies of one and three plates, respectively,
 270 whose declared $^{40}\text{Pu}_{\text{eff}}$ masses were 4.70 ± 0.02 g and 23.50 ± 0.02 g, respectively. For comparison to the
 271 currently used thermal systems, the High Level Neutron Coincidence Counter II (HLNCC-II) is able to
 272 estimate a $^{40}\text{Pu}_{\text{eff}}$ mass of 9.70 ± 0.39 g (4.0% relative uncertainty) for a plutonium metal sample of 9.39-g
 273 declared $^{40}\text{Pu}_{\text{eff}}$ mass, in 5.5 minutes [6]. A lower percent uncertainty of 1.3% is achieved for the same
 274 sample in the HLNCC-II by increasing the assay time to 110 minutes. The HLNCC-II consists of a single
 275 ring of 18 cylindrical ^3He proportional detectors (2.5 cm diameter by 50 cm length) filled to a pressure of
 276 4 atm.

277 **Table 3. Estimated $^{240}\text{Pu}_{\text{eff}}$ mass using the single-parameter calibration method.**

PAHN							
Number of plates	1	5	7	11	13	17	19
Actual ^{240}Pu effective mass (g)	25.05	125.23	175.32	275.51	325.60	425.79	475.88
Estimated ^{240}Pu effective mass (g)	24.92 ± 0.49	124.98 ± 1.13	177.10 ± 1.08	276.99 ± 0.74	326.75 ± 0.66	422.30 ± 1.09	470.53 ± 1.49
Absolute bias (g)	-0.12	-0.25	1.78	1.48	1.15	-3.49	-5.35
PANN							
Number of plates	1	5	7	11	13	17	19
Actual ^{240}Pu effective mass (g)	4.70	23.50	32.90	51.71	61.11	79.91	89.31
Estimated ^{240}Pu effective mass (g)	4.78 ± 0.10	23.43 ± 0.24	32.45 ± 0.22	51.48 ± 0.16	61.46 ± 0.15	80.25 ± 0.21	88.79 ± 0.26
Absolute bias (g)	0.08	-0.07	-0.46	-0.22	0.35	0.34	-0.52

278

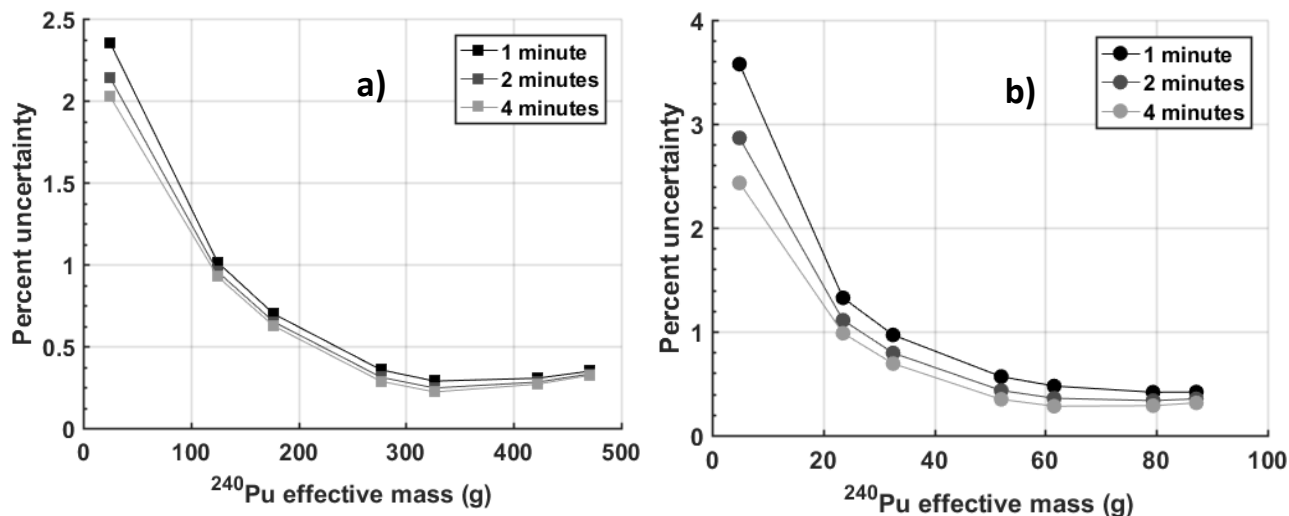


Figure 9. Statistical percent uncertainty as a function of $^{240}\text{Pu}_{\text{eff}}$ mass for increasing assay times, for PAHN (a) and PANN plates (b).

279 3.4 Comparison of EJ-309 and stilbene detectors in terms of measurement precision

280 We have evaluated the contribution to the overall measurement uncertainty given by 8 EJ-309 and 8
 281 stilbene detectors, considered as two separate arrays. Measurement uncertainty is affected by two
 282 main components, the counting statistics (first term in Eq. 4) and the goodness of the fitted model
 283 (second, third and fourth term in Eq. 4). We analyzed these contributions separately, for stilbene and EJ-
 284 309 detectors for a 4-minute assay of the PANN plate series (Fig. 10).

285 In this case, the uncertainty is dominated by the counting statistics component (Fig. 10). For this reason,
 286 the array of EJ-309 detectors yields an overall lower uncertainty, because of the larger volume and thus
 287 higher intrinsic efficiency of EJ-309 detectors, compared to stilbene crystals.

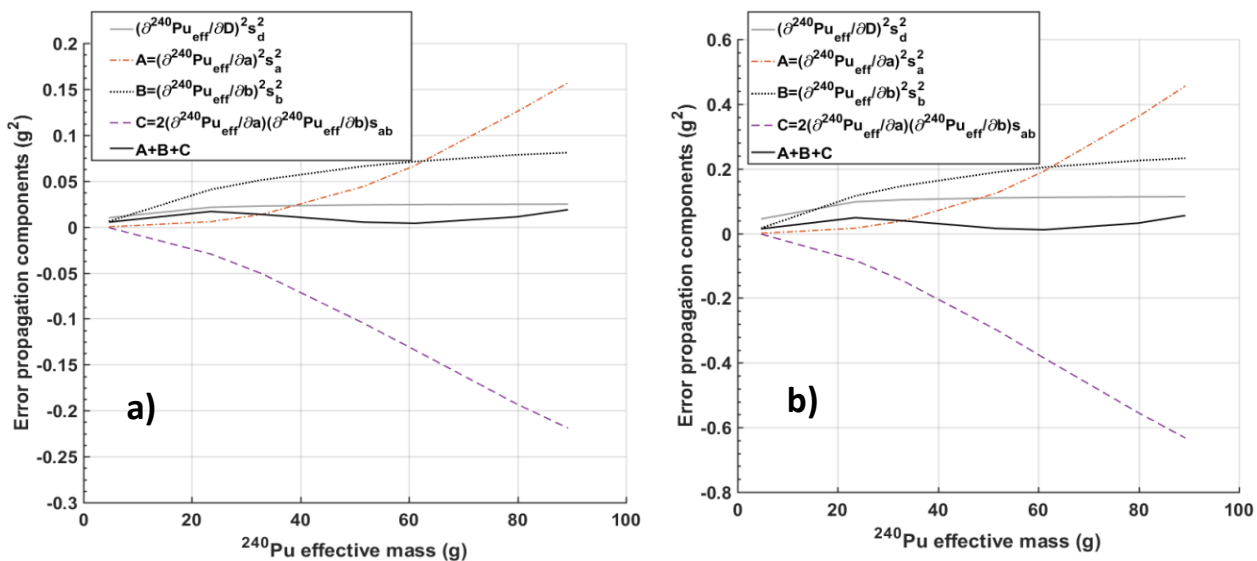


Figure 10. Components of the error propagation (Eq. 4), as a function of $^{240}\text{Pu}_{\text{eff}}$ mass, for pairs of EJ-309 (a) and stilbene detectors (b), for PANN plates and a measurement time of 10 minutes. The solid and black grey lines show the counting statistics and goodness of the fit contributions to the overall uncertainty, respectively.

288
 289
 290

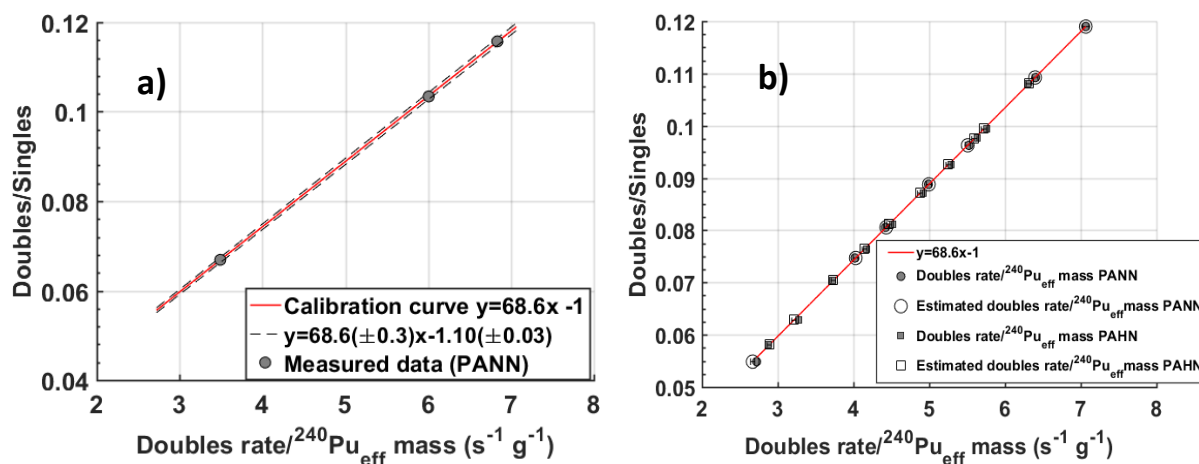
291 Table 4. Comparison of estimated $^{240}\text{Pu}_{\text{eff}}$ mass and its uncertainty by using EJ-309 and stilbene detectors separately, for
 292 PAHN plates.

Number of plates	1	5	9	11	15	17	19
Actual ^{240}Pu effective mass (g)	25.05	125.23	225.42	275.51	375.69	425.79	475.88
Estimated ^{240}Pu effective mass – stilbene array (g)	24.97 ± 0.57	125.98 ± 0.99	178.03 ± 1.05	277.59 ± 1.11	327.81 ± 1.13	428.00 ± 1.15	478.10 ± 1.18
Estimated ^{240}Pu effective mass – EJ-309 array (g)	24.95 ± 0.74	124.62 ± 1.68	176.75 ± 1.60	276.96 ± 1.14	326.57 ± 1.04	422.20 ± 1.60	473.70 ± 2.12

293
 294 The uncertainty contribution due to counting statistics becomes negligible when assaying samples with
 295 activity higher than PANN, or by increasing the measurement time. As we verified for PAHN plates
 296 (Table 4), when the number of measured doubles exceeds approximately 25,000, the main source of
 297 uncertainty becomes the third term in Eq. 4, which depends on the rate of neutron doubles, the
 298 coefficients a and b and the variance, s^2_b . We found that in these conditions the $^{240}\text{Pu}_{\text{eff}}$ mass was
 299 estimated more precisely by the array of stilbene crystals than EJ-309 detectors, mainly due to a more
 300 precise estimate of the b coefficient, whose uncertainty was 0.5% and 3.1% for stilbene and EJ-309
 301 detectors, respectively.

302
 303 **3.5 Estimate of ^{240}Pu effective mass using two-parameter calibration**

304 We used PANN assemblies of 3, 13 and 17 plates as calibration set to test the two-parameter calibration
 305 method. As expected, the ratio between double and single neutrons for both sets of plates is well
 306 described by a linear relationship as a function of the neutron doubles rate per unit $^{240}\text{Pu}_{\text{eff}}$ mass (Fig.
 307 11).



308 Figure 11. Two-parameter calibration (a) and assay (b).

309 We were able to measure in singles mode most of the assemblies of PANN plates. We used instead the
 310 simulated neutron singles when measured data were not available, e.g., in the case of highly radioactive
 311 PAHN samples acquired in coincidence mode. The combined standard uncertainty associated with the
 312 $^{240}\text{Pu}_{\text{eff}}$ mass estimated with this method was comparable to the one achieved by the single-parameter
 313 calibration method (Table 5). The absolute bias was negligible for test samples of the same type of the
 314 calibration test series, i.e. PANN plates, while in general higher, in absolute value, than the bias error of
 315 the single-parameter calibration procedure.

316 **Table 5. Estimated $^{240}\text{Pu}_{\text{eff}}$ mass using the two-parameter calibration method.**

PAHN										
Number of plates	1	3	5	7	9	11	13	15	17	19
Actual ^{240}Pu effective mass (g)	25.05	75.14	125.23	175.32	225.42	275.51	325.60	375.69	425.79	475.88
Estimated ^{240}Pu effective mass (g)	24.90 ± 0.35	76.66 ± 0.21	124.96 ± 0.19	176.34 ± 0.17	227.75 ± 0.16	277.66 ± 0.14	327.65 ± 0.13	378.49 ± 0.04	428.98 ± 0.04	474.73 ± 0.04
Absolute bias (g)	-0.15	1.52	-0.27	1.02	2.33	2.15	2.05	2.80	3.20	-1.15
PANN										
Number of plates	1	3	5	7	9	11	13	15	17	19
Actual ^{240}Pu effective mass (g)	4.70		23.50	32.90	42.31	51.71		70.51		89.31
Estimated ^{240}Pu effective mass (g)	4.70 ± 0.34	n. a.	23.50 ± 0.21	32.90 ± 0.19	42.31 ± 0.17	51.71 ± 0.16	n. a.	70.51 ± 0.14	n. a.	89.31 ± 0.13
Absolute bias (g)	< 0.001		< 0.001	< 0.001	< 0.001	< 0.001		< 0.001		< 0.001

317

318

319

320 **4. Summary and conclusions**

321 We designed and developed a fast-neutron multiplicity counter based on 8 EJ-309 liquid and 8 stilbene
 322 crystal detectors. The system geometry was optimized for the passive assay of plutonium metal samples
 323 of different composition. Two types of plutonium metal plates, with different ^{240}Pu effective mass, were
 324 used at Idaho National Laboratory: PAHN and PANN (4.7 g and 25.05 g $^{240}\text{Pu}_{\text{eff}}$ mass per plate,
 325 respectively). The ^{239}Pu mass percentage was 74% for the PAHN and 95% for the PANN series. We
 326 measured neutrons emitted in coincidence by several plate assemblies, having an overall ^{240}Pu effective
 327 mass from 4.7 g to 476 g.

328 The stilbene detectors proved to be suitable for this application, as their excellent PSD capability allows
 329 operating them at a neutron detection threshold of approximately 350 keV. This energy threshold is
 330 lower compared to the 520 keV threshold required for the EJ-309 liquid scintillators to effectively
 331 discriminate neutrons from gamma-rays. Because of the low energy threshold, the stilbene effective
 332 response, i.e., normalized by detector volume and solid angle, was constantly higher than the EJ-309
 333 liquid response by about 50%.

334 The system was operated in coincidence mode and two calibration-based approaches were used to
335 estimate the $^{240}\text{Pu}_{\text{eff}}$ mass of the samples. Both methods succeeded in estimating the $^{240}\text{Pu}_{\text{eff}}$ mass of an
336 unknown sample with an uncertainty lower than 1% in a 4-minute assay time ($^{240}\text{Pu}_{\text{eff}} > 50$ g). The
337 statistical uncertainty is lower than the one achieved by standard ^3He counters for plutonium metal
338 samples of similar mass. The difference between the estimated and the declared $^{240}\text{Pu}_{\text{eff}}$ mass, i.e., the
339 bias error, measured by the fast neutron multiplicity counter was consistently lower compared to the
340 bias error of a standard thermal system.

341 The first calibration method related the neutron coincidence rate with the $^{240}\text{Pu}_{\text{eff}}$ mass, so it is specific
342 for samples of a given composition and multiplication. The second method related the doubles/singles
343 neutron ratio to the doubles rate per unit $^{240}\text{Pu}_{\text{eff}}$ mass, and is virtually independent of the plutonium
344 isotopic composition and multiplication, as long as the (α, n) neutron component is the same for the
345 samples to be assayed. This second approach, although slightly less accurate than the first one, may be
346 useful whenever the isotopic composition of the calibration series is different from the composition of
347 the test series.

348 By evaluating stilbene and EJ-309 detectors separately, as if they were virtually two separate systems,
349 the stilbene-based counter outperformed the EJ-309-based counter in terms of measurement precision,
350 as long as at least 25,000 neutron doubles were detected, i.e., the measurement uncertainty became
351 negligible compared to the uncertainty associated with the capability of the adopted model to explain
352 the measured data.

353 Further work is needed to assess potential limitations of the systems, such as operational drifts due to
354 external temperature caused by the temperature dependence of the gain of photomultiplier tubes. In
355 this work, spurious coincidences due to cross-talk were minimized by rejecting counts from nearest
356 neighbor detectors, however new algorithms are being developed which are able to account for those
357 events in the general framework of the multiplicity analysis equations. A promising property of the
358 system is its position sensitivity, which will be further investigated and could be used to improve the
359 characterization of unknown samples by measuring the known angular distribution of neutrons emitted
360 by ^{240}Pu spontaneous fission [23].

361 **Acknowledgements**

362
363 The authors thank the staff at the ZPPR facility of Idaho National Laboratory for their assistance during
364 the measurement campaign. This work is funded in-part by the Consortium for Verification Technology
365 under Department of Energy National Nuclear Security Administration award number DE-NA0002534.
366

367 **References**

- 368 [1] M.S. Krick, J.E. Swansen, Neutron multiplicity and multiplication measurements, Nucl. Instr.
369 Meth. Phys. Res. 219 (1984) 384–393.
- 370 [2] R.T. Kouzes, J.H. Ely, A.T. Lintereur, E.K. MacE, D.L. Stephens, M.L. Woodring, Neutron detection
371 gamma ray sensitivity criteria, Nucl. Instr. Meth. Phys. Res. A. 654 (2011) 412–416.

- 372 [3] S.M. Robinson, R.C. Runkle, R.J. Newby, A comparison of performance between organic
373 scintillation crystals and moderated ^3He -based detectors for fission neutron detection, *Nucl.*
374 *Instr. Meth. Phys. Res. A.* 652 (2011).
- 375 [4] H. Menlove, J. Stewart, S. Qiao, T. Wenz, P. Verrecchia, Neutron Collar Calibration and Evaluation
376 for Assay of LWR Fuel Assemblies Containing Burnable Neutron Absorbers, n.d.
- 377 [5] G.F. Knoll, *Radiation Detection and Measurement*, 4th ed., John Wiley & Sons, Inc., Hoboken,
378 2011.
- 379 [6] D. Henzlova, R. Kouzes, R. McElroy, P. Peerani, K. Baird, A. Bakel, M. Borella, M. Bourne, L.
380 Bourva, F. Cave, R. Chandra, D. Chernikova, S. Croft, G. Dermody, A. Dougan, J. Ely, E. Fanchini, P.
381 Finocchiaro, V. Gavron, M. Kureta, K.D. Ianakiev, K. Ishiyama, T. Lee, C. Martin, K. McKinny, H.O.
382 Menlove, C. Orton, A. Pappalardo, B. Pedersen, R. Plenteda, S. Pozzi, M. Shear, M. Seya, E.
383 Siciliano, S. Stave, L. Sun, M.T. Swinhoe, H. Tagziria, J. Takamine, A.-L. Weber, T. Yamaguchi, H.
384 Zhu, *Current Status of Helium-3 Alternative Technologies for Nuclear Safeguards*, 2015.
- 385 [7] D.L. Chichester, S.J. Thompson, M.T. Kinlaw, J.T. Johnson, J.L. Dolan, M. Flaska, S.A. Pozzi,
386 Statistical estimation of the performance of a fast-neutron multiplicity system for nuclear
387 material accountancy, *Nucl. Instr. Meth. Phys. Res. A.* 784 (2015) 448–454.
- 388 [8] E. Technology, NEUTRON/GAMMA PSD LIQUID SCINTILLATOR EJ-301, EJ-309, (n.d.).
389 http://www.eljentechnology.com/images/products/data_sheets/EJ-301_EJ-309.pdf (accessed
390 May 12, 2016).
- 391 [9] N. Zaitseva, A. Glenn, L. Carman, H. Paul Martinez, R. Hatarik, H. Klapper, S. Payne, Scintillation
392 properties of solution-grown trans-stilbene single crystals, *Nucl. Instr. Meth. Phys. Res. A.* 789
393 (2015).
- 394 [10] N.Z. Galunov, O.A. Tarasenko, V.A. Tarasov, Determination of the light yield of organic
395 scintillators, *Funct. Mater.* 20 (2013).
- 396 [11] CAEN S.p.A., V1730 user manual, (2016).
- 397 [12] J.K. Polack, M. Flaska, A. Enqvist, C.S. Sosa, C.C. Lawrence, S.A. Pozzi, An algorithm for charge-
398 integration, pulse-shape discrimination and estimation of neutron/photon misclassification in
399 organic scintillators, *Nucl. Instr. Meth. Phys. Res. A.* 795 (2015) 253–267.
- 400 [13] J.B. Briks, *The Theory and Practice of Scintillation Counting*, Pergamon, Oxford, 1964.
- 401 [14] D. Reilly, N. Ensslin, H. Smith, eds., *Passive Nondestructive Assay Manual - PANDA*, Los Alamos
402 National Laboratory, 1991.
- 403 [15] T.H. Shin, M.J. Marath, A. Di Fulvio, S.D. Clarke, S.A. Pozzi, Neutron cross-talk characterization of
404 liquid organic scintillators, in: *2015 IEEE Nucl. Sci. Symp. Med. Imaging Conf. NSS/MIC 2015*,
405 2016.
- 406 [16] M.A. Norsworthy, A. Poitrasson-Rivière, M.L. Ruch, S.D. Clarke, S.A. Pozzi, Evaluation of neutron
407 light output response functions in EJ-309 organic scintillators, *Nucl. Instr. Meth. Phys. Res. A.* 842
408 (2016) 20–27.

- 409 [17] M. Norsworthy, M.M. Bourne, Personal communication, (2016).
- 410 [18] D.L. Chichester, Properties of Nuclear Fuel Used in Tests with the LLNL Gamma-Ray Mirror in
411 September 2014, 2014.
- 412 [19] C.W. Solbrig, J. Andrus, C. Pope, ZPPR Fuel Element Thermal Stress-Strain Analysis, World J. Nucl.
413 Sci. Technol. 4 (2014).
- 414 [20] J.L. Dolan, M. Flaska, A. Poitrasson-Riviere, A. Enqvist, P. Peerani, D.L. Chichester, S.A. Pozzi,
415 Plutonium measurements with a fast-neutron multiplicity counter for nuclear safeguards
416 applications, Nucl. Instr. Meth. Phys. Res. A. 763 (2014) 565–574.
- 417 [21] G. Cowan, Statistical Data Analysis, 1st ed., Clarendon Press, Oxford, 1998.
- 418 [22] S.A. Pozzi, S.D. Clarke, W.J. Walsh, E.C. Miller, J.L. Dolan, M. Flaska, B.M. Wieger, A. Enqvist, E.
419 Padovani, J.K. Mattingly, D.L. Chichester, P. Peerani, MCNPX-PoliMi for nuclear nonproliferation
420 applications, Nucl. Instr. Meth. Phys. Res. A. 694 (2012) 119–125.
- 421 [23] M.J. Marcath, T.H. Shin, S.D. Clarke, P. Peerani, S.A. Pozzi, Neutron angular distribution in
422 plutonium-240 spontaneous fission, Nucl. Instr. Meth. Phys. Res. A. 830 (2016).
- 423